Sensors and Actuators A 149 (2009) 74–80

Contents lists available at ScienceDirect

Sensors and Actuators A: Physical

journal homepage: www.elsevier.com/locate/sna

Calibration and on-line data selection of multiple optical flow sensors for odometry applications

Jwu-Sheng Hu, Yung-Jung Chang*, Yu-Lun Hsu

Department of Electrical and Control Engineering, National Chiao Tung University, Hsinchu 300, Taiwan, ROC

ARTICLE INFO

Article history:
Received 15 May 2008
Received in revised form 12 August 2008
Accepted 12 October 2008
Available online 21 October 2008

Keywords:
Optical flow sensor
Optical mouse
Odometry
Multiple sensors
Calibration
Data selection

ABSTRACT

This work proposes a calibration method and a computational algorithm to integrate the data of multiple optical flow sensors for two-dimensional trajectory measurements. Optical flow sensors offer a different kind of odometer as compared to the wheel encoder. Using multiple sensors can reduce the effect of measurement uncertainties. Since all sensors are mounted on a rigid body, their measurement data must obey a certain relation, which is utilized in this work. Additionally, mathematical formulae are developed to realize the computation. Analytical results show that the calibration procedure can be cast as an optimization problem given measurement data. Furthermore, the rigid-body relation is formulated as a null-space constraint using the calibrated parameters. Unreliable sensor measurements can be removed during operation by accessing the error distance to the null space. Experimental results are presented to support the proposed methods.

1. Introduction

Localizing a mobile robot in an indoor environment is an important issue in robotics. The position estimation methods can be classified into two basic categories, namely absolute and relative positioning [1]. Common absolute positioning technologies include GPS, navigation beacons, map-matching and landmarks while relative positioning systems include odometers or inertial sensors. Different sensors can be combined to alleviate the shortcomings of individual sensors. However, increasing the accuracy of one sensor is fundamental to enhancing the accuracy of localization.

Odometers based on wheel encoders are most commonly used in practice because of their simplicity and availability. Localization using optical flow sensors (or optical mouse sensor) has recently been proposed [3–10]. Odometer measurements have also been combined with landmarks to perform self-localization [6,11]. Unlike wheel encoder, the optical flow sensor measurement is not affected by wheel-slippage, because of direct sensing of the movement between the sensor and sensing surface. Moreover, the cost of the sensor is low, due to the wide usage of computer mice. Off-the-shelf optical flow sensors with resolutions of 2000 counts per inch are now easy to obtain.

An optical mouse utilizes a miniaturized CMOS camera to capture consecutive images reflected from the surface through LED illumination. The camera, LED and associated optical mechanism are arranged to ensure a robust measurement [9]. Because the surface has texture variation, the sensor can detect the motion of the sensor by matching the patterns between consecutive images (e.g., autocorrelation [12]). Although both translational and rotational measurements can be obtained, off-the-shelf sensors only give translation information, because rotation is not required in computer mouse applications. Therefore, at least two optical flow sensors have to be employed to detect the complete motion information [4–8].

Many factors might affect the accuracy of the optical flow measurement. Palacin et al. [9] analyzed in detail the possible errors of the optical flow sensor itself. These errors can be reduced by averaging the measurements over an array of sensors. However, taking the average does not consider the differences among the sensors as they might encounter different conditions. For instance, an optical flow sensor passing by a hole (i.e., a sudden change of height of the surface) gives an incorrect reading because it goes out of focus. Moreover, other issues need to be considered when adopting multiple sensors. Borenstein and Feng [2] categorized the errors as systematic and non-systematic. In this work, the factors leading to the systematic errors include imperfect position and orientation arguments of optical flow sensors, and varying resolutions. Conversely, the non-systematic errors come from the sensor itself, and include the inability to detect the change of a homogeneous surface

* Corresponding author. Tel.: +886 3 5712121.
E-mail address: rednuo@gmail.com (Y.-J. Chang).

0924-4247/$ – see front matter © 2008 Elsevier B.V. All rights reserved.
doi:10.1016/j.sna.2008.10.003

as well as the excessive distance between the sensor and sensing surface [7].

These technical issues mentioned above have never been studied in detail when constructing a sensor module using multiple optical flow sensors. This work proposes a calibration method to eliminate the systematic errors, and a consistency check strategy to reduce the inaccuracy resulting from non-systematic errors. The underlying principle is similar to sensor fusion, in which the readings of all sensors must reflect the fact that they are mounted under a rigid body. Rigorous mathematical formulations and derivations are presented to facilitate the practical design. The next section describes the integration of multiple optical flow sensors. Section 3 introduces the rigid-body constraints and the geometric relations of optical flow sensors. Section 4 presents the calibration method, which optimizes the parameters of sensors using the formulation in Section 3. Section 5 describes the consistency check strategy, which selects the reliable sensor measurements during operation. Experimental results are given in Section 6, and conclusions are drawn in Section 7.

2. Position and orientation estimation using multiple sensors

This section extends the pose estimation method of two sensors in Ref. [7] to multiple sensors. Consider a system with N optical flow sensors, labeled as $i = 1$ to N, mounted on a plane. Each sensor can measure a two-dimensional translation in its own coordinates. Sensor coordinates (coordinate defined on the motion detection axes of the optical flow sensor) are generally not necessary aligned with each other. Suppose that two sensors i and j (Fig. 1) are at a distance D_{ij} to each other. The coordinate of sensor i is rotated at the angle σ_{ij} relative to the line connecting both sensors (line $\overline{O_iO_j}$ in Fig. 1) while the angle for sensor j is σ_{ji}. The signs of σ_{ij} and σ_{ji} are positive if the rotation is counterclockwise (CCW) and negative otherwise.

Considering that the sensors move along an arc during the sampling interval, the length of the arc is approximated as,

$$l_i = \sqrt{\bar{x}_i^2 + \bar{y}_i^2} \tag{1}$$

where $\bar{x}_i$ and $\bar{y}_i$ denote the measurements of sensor i at each sample instance on the coordinate of sensor i. The motion direction (tangent to the arc) of sensor i is at the angle σ_i relative to the sensor coordinate, i.e.

$$l_i \cos(\alpha_i) = \bar{x}_i \text{ and } l_i sin(\alpha_i) = \bar{y}_i. \tag{2}$$

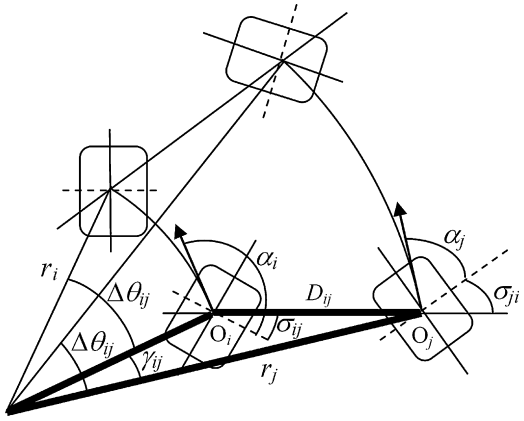

Fig. 1. Geometric relation of two sensors.

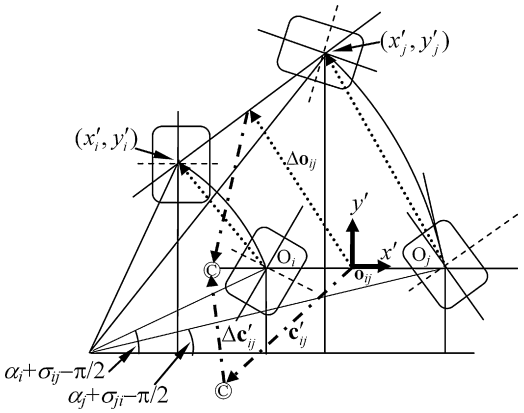

Fig. 2. The movement within a sampling interval of two sensors.

From Fig. 1, the angle γ_{ij} can be calculated as $\gamma_{ij} = |\alpha_i + \sigma_{ij} - \alpha_j - \sigma_{ij}|$. Denoting the rotational angle as $\Delta\theta_{ij}$, the radius of rotation for sensor i is,

$$r_i = \frac{l_i}{\Delta\theta_{ij}} \tag{3}$$

Additionally, from the cosine law, $\Delta\theta_{ij}$ can be calculated as,

$$\Delta\theta_{ij} = \frac{\sqrt{l_i^2 + l_j^2 - 2\cos(\gamma_{ij}) l_i l_j}}{D_{ij}} sign(l_j \sin(\alpha_j + \sigma_{ji}) - l_i \sin(\alpha_i + \sigma_{ij})) \tag{4}$$

Define a coordinate (x', y') aligned with the line $\overline{O_iO_j}$ and the origin located at its mid-point (Fig. 2). The new sensor locations can be calculated as,

$$x'_i = r_i(\sin(\Delta\theta_{ij} + \alpha_i + \sigma_{ij}) - \sin(\alpha_i + \sigma_{ij}))sign(\Delta\theta_{ij}) + D_{ij}/2 \tag{5a}$$

$$y'_i = r_i(\cos(\alpha_i + \sigma_{ij}) - \cos(\Delta\theta_{ij} + \alpha_i + \sigma_{ij}))sign(\Delta\theta_{ij}) \tag{5b}$$

$$x'_j = r_j(\sin(\Delta\theta_{ij} + \alpha_j + \sigma_{ji}) - \sin(\alpha_j + \sigma_{ji}))sign(\Delta\theta_{ij}) - D_{ij}/2 \tag{5c}$$

$$y'_j = r_j(\cos(\alpha_j + \sigma_{ji}) - \cos(\Delta\theta_{ij} + \alpha_j + \sigma_{ji}))sign(\Delta\theta_{ij}) \tag{5d}$$

Denoting the center of the line $\overline{O_iO_j}$ as $\mathbf{o}_{ij}$ and its movement as $\Delta\mathbf{o}_{ij}$ (see Fig. 2), we have,

$$\Delta\boldsymbol{o}_{ij}[\Delta x'_{ij} \quad \Delta y'_{ij}]^T \tag{6}$$

where

$$\Delta x'_{ij} = \frac{(x'_i + x'_j)}{2} \quad \text{and} \quad \Delta y'_{ij} = \frac{(y'_i + y'_j)}{2}.$$

If the center of the robot relative to the $\mathbf{o}_{ij}$ on the coordinate of Fig. 2 is given by $\boldsymbol{c}'_{ij}$, the movement of the center, denoted as $\Delta\boldsymbol{c}'_{ij}$, is

$$\Delta\boldsymbol{c}'_{ij} = (\boldsymbol{T}(\Delta\theta_{ij}) - \boldsymbol{I})\boldsymbol{c}'_{ij} + \Delta\boldsymbol{o}_{ij} \tag{7}$$

where $\mathbf{I}$ is the identity matrix and $\mathbf{T}(\Delta\theta_{ij})$ is the transformation matrix, given by

$$\boldsymbol{T}(\Delta\theta_{ij}) = \begin{bmatrix} \cos(\Delta\theta_{ij}) & -\sin(\Delta\theta_{ij}) \\ \sin(\Delta\theta_{ij}) & \cos(\Delta\theta_{ij}) \end{bmatrix} \tag{8}$$

Secondly, if the orientation of the vector $\vec{O_iO_j}$ to the robot coordinate is given by β_{ij}, the movement represented by the robot coordinate (denoted as $\Delta\mathbf{c}_{ij}$) is

$$\Delta\boldsymbol{c}_{ij} = \boldsymbol{T}(\beta_{ij})\Delta\boldsymbol{c}'_{ij} \tag{9}$$

Therefore, the robot position and orientation relative to the global coordinate computed from the sensor pair i, j at time $k+1$ are

$$\theta(k+1) = \theta(k) + \Delta\theta_{ij} \tag{10}$$

$$\boldsymbol{c}(k+1) = \boldsymbol{c}(k) + \boldsymbol{T}(\theta(k))\Delta\boldsymbol{c}_{ij} \tag{11}$$

For N sensors, there will be $C_2^N = N(N-1)/2$ solutions to update the robot position and orientation. The update can be conducted straightforwardly by computing the mean as,

$$\theta(k+1) = \theta(k) + \frac{2}{N(N-1)}\sum_{i=1}^{N-1}\sum_{j=i+1}^{N}\Delta\theta_{ij} \tag{12}$$

$$\boldsymbol{c}(k+1) = \boldsymbol{c}(k) + \frac{2}{N(N-1)}\boldsymbol{T}(\theta(k))\sum_{i=1}^{N-1}\sum_{j=i+1}^{N}\Delta\boldsymbol{c}_{ij} \tag{13}$$

3. The rigid-body constraints and geometric relations among sensors

Since all sensors are fixed relative to each other, the measurements must obey the rigid-body constraint. This constraint can be applied to perform calibration, as well as to determine the correctness of measurement. For rigid-body motion, the constraint between any two sensors according to Fig. 1 is given by

$$l_i\cos(\alpha_i + \sigma_{ij}) = l_j\cos(\alpha_j + \sigma_{ji}) \tag{14}$$

or

$$l_i\cos(\alpha_i)\cos(\sigma_{ij}) - l_i\sin(\alpha_i)\sin(\sigma_{ij}) = l_j\cos(\alpha_j)\cos(\sigma_{ji}) - l_j\sin(\alpha_j)\sin(\sigma_{ji}). \tag{15}$$

This means that the sensor measurements projected onto the joining line in Fig. 1 should all be the same. For N sensors, there are $N(N-1)/2$ constraint equations. Since $l_i\cos(\alpha_i) = \bar{x}_i$ and $l_i\sin(\alpha_i) = \bar{y}_i$, where $\bar{x}_i$ and $\bar{y}_i$ are the sensor measurements during each sampling interval on the sensor coordinate, the equation becomes

$$\bar{x}_i\cos(\sigma_{ij}) - \bar{y}_i\sin(\sigma_{ij}) - \bar{x}_{ij}\cos(\sigma_{ji}) - \bar{y}_j\sin(\sigma_{ji}) \tag{16}$$

However, this equation cannot hold for incorrect values of σ_{ij}, or disturbed sensor measurements. Consequently, the equation error of (16) can be defined as

$$\varepsilon_{ij} = \bar{x}_i\cos(\sigma_{ij}) - \bar{y}_j\sin(\sigma_{ij}) - \bar{x}_j\cos(\sigma_{ji}) + \bar{y}_j\sin(\sigma_{ji}) \tag{17}$$

ε_{ij} can be used to determine the correctness of the nominal parameters and the reliability of the sensor reading. Define the error vector ε as the collection of $N(N-1)/2$ errors ε_{ij},

$$\boldsymbol{\varepsilon} = [\varepsilon_{12} \quad \varepsilon_{13} \quad \dots \quad \varepsilon_{(N-1)N}]^T = \mathbf{B}\cdot X \tag{18}$$

where $\mathbf{B}$ indicates a matrix of dimension $N(N-1)/2 \times 2N$ defined as

$$\mathbf{B} = \begin{bmatrix} \cos(\sigma_{12}) & -\sin(\sigma_{12}) & -\cos(\sigma_{21}) & \sin(\sigma_{21}) & 0 & 0 & \dots & \dots & \dots & \dots & 0 \\ \cos(\sigma_{13}) & -\sin(\sigma_{13}) & 0 & 0 & -\cos(\sigma_{31}) & \dots \sin(\sigma_{31}) & \dots & \dots & \dots & \dots & 0 \\ \vdots & \vdots & \vdots & \vdots & \vdots & \vdots & \vdots & \vdots & \vdots & \vdots & \vdots \\ 0 & 0 & 0 & 0 & 0 & 0 & \dots & \cos(\sigma_{(N-1)N}) & -\sin(\sigma_{(N-1)N}) & -\cos(\sigma_{N(N-1)}) & \sin(\sigma_{N(N-1)}) \end{bmatrix} \tag{19}$$

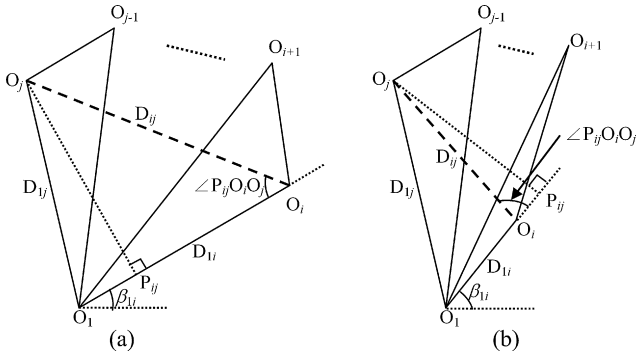

Fig. 3. The geometric relations of angles: (a) acute angle case; (b) obtuse angle case.

and $X = [\bar{x}_1 \quad \bar{y}_1 \quad \bar{x}_2 \quad \bar{y}_2 \quad \cdots \quad \bar{x}_N \quad \bar{y}_N]^T$ is the vector of sensor measurements with dimension $2N \times 1$. Moreover, if the orientation of the sensors i and j to the robot coordinate are given as ϕ_i and ϕ_j, respectively, the angles σ_{ij} and σ_{ji} can be derived as $\sigma_{ij} = \phi_i - \beta_{ij}$ and $\sigma_{ji} = \phi_j - \beta_{ij}$.

Eq. (18) is used to compute the parameters in $\mathbf{B}$ by minimizing the norm of $\boldsymbol{\varepsilon}$. $\mathbf{B}$ contains the angular parameters of sensors, i.e. all ϕ_i's and β_{ij}'s. The number of ϕ_i values is N, and the number of β_{ij} values is $N(N-1)/2$ (since $\beta_{ji} = \beta_{ij} + \pi$ and no β_{ii} exists). Further, all ϕ_i's are independent of each other, while β_{ij}'s are not. Thus, certain relations among β_{ij}'s must to be satisfied when performing the minimization. Initially, define the coordinate of sensor 1 as the robot coordinate, and the center of sensor 1 as the origin, i.e. $\phi_1 = 0$, and the position of sensor 1 is (0,0). Fig. 3 shows the relations among sensors 1, i, $i+1$, j and $j-1$. Two cases may be found when computing β_{ij}.

In Fig. 3, suppose that $\overline{P_{ij}O_i}$ is perpendicular to $\overline{O_iO_j}$, and that point P_{ij} is a point on line $\overline{O_iO_j}$. In the first case (Fig. 3(a)), $\angle P_{ij}O_iO_j$ is an acute angle, and clearly, the angle $\beta_{ij} = \beta_{1i} + (\pi - \angle P_{ij}O_iO_j)$. Let $\psi_{a,b,c}$ denote the notation of angle $\angle O_aO_bO_c$, and D_{ij} denote the length of $\overline{O_iO_j}$. Clearly, the length of $\overline{P_{ij}O_j}$ is equal to $D_{1j}\sin(\psi_{i,1,j})$, and the length of $\overline{P_{ij}O_i}$ is equal to $D_{1i} - D_{1j}\cos(\psi_{i,1,j})$. Consequently, the angle $\angle P_{ij}O_iO_j$ is given by

$$\angle P_{ij}O_iO_j = \arctan\left(\frac{D_{1j}\sin(\psi_{i,1,j})}{D_{1i} - D_{1j}\cos(\psi_{i,1,j})}\right) \tag{20}$$

and according to the cosine law,

$$D_{1i} = \frac{\sin(\psi_{1,i+1,i})\sin(\psi_{1,i+2,i+1})\cdots\sin(\psi_{1,j,j-1})}{\sin(\psi_{1,i,i+1})\sin(\psi_{1,i+1,i+2})\cdots\sin(\psi_{1,j-1,j})}D_{1j} \tag{21}$$

Hence,

$$\angle P_{ij}O_iO_j = \arctan\left(\frac{\sin(\psi_{i,1,j})}{\sin(\psi_{1,i+1,i})\sin(\psi_{1,i+2,i+1})\cdots\sin(\psi_{1,j,j-1})/\sin(\psi_{1,i,i+1})\sin(\psi_{1,i+1,i+2})\cdots\sin(\psi_{1,j-1,j}) - \cos(\psi_{i,1,j})}\right) \tag{22}$$

In the second case (Fig. 3(b)), the angle $\angle P_{ij}O_iO_j$ is an obtuse angle and $\beta_{iij} = \beta_{1i} + \angle P_{ij}O_iO_j$. The following equation is obtained.

$$\angle P_{ij}O_iO_j = \arctan\left(\frac{\sin(\psi_{i,1,j})}{\cos(\psi_{i,1,j}) - (\sin(\psi_{1,i+1,i})\sin(\psi_{1,i+2,i+1})\cdots\sin(\psi_{1,j,j-1}))/(\sin(\psi_{1,i,i+1})\sin(\psi_{1,i+1,i+2})\cdots\sin(\psi_{1,j-1,j}))}\right) \tag{23}$$

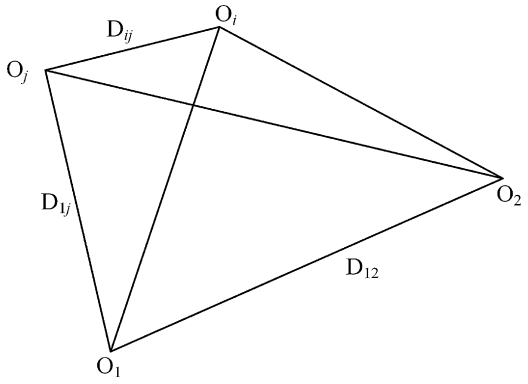

Fig. 4. Geometric relations of the lengths.

It is easy to verify that $\psi_{i,1,j} = \beta_{1j} - \beta_{1i}$, $\psi_{1,i,i+1} = \pi - (\beta_{ii+1} - \beta_{1i})$, $\psi_{1,i+1,i} = \beta_{ii+1} - \beta_{1i+1}$, $\psi_{1,i+1,i+2} = \beta_{i+1i+2} - \beta_{1i+1}$, $\psi_{1,i+2,i+1} = \pi - (\beta_{i+1\,i+2} - \beta_{1\,i+2})$, and so on. Therefore, the equation for angle β_{ij} can be recast as,

$$\beta_{ij} = \begin{cases} \beta_{1i} + \pi - \arctan(\sin(\beta_{1j} - \beta_{1i})/S_{ij} - \cos(\beta_{1j} - \beta_{1i})), & \text{case (a)} \\ \beta_{1i} + \arctan(\sin(\beta_{1j} - \beta_{1i})/\cos(\beta_{1j} - \beta_{1i}) - S_{ij}), & \text{case (b)} \end{cases} \tag{24}$$

where

$$S_{ij} = \frac{\sin(\beta_{i\,i+1} - \beta_{1\,i+1})\sin(\beta_{i+1\,i+2} - \beta_{1\,i+2}) \cdots \sin(\beta_{j-1\,j} - \beta_{1j})}{\sin(\beta_{i\,i+1} - \beta_{1\,i})\sin(\beta_{i+1\,i+2} - \beta_{1\,i+1}) \cdots \sin(\beta_{j-1\,j} - \beta_{1\,j-1})}$$

Eq. (24) shows the relationship among β_{ij} values, clearly revealing that the free parameters are β_{1j}, $j = 2$ to N and $\beta_{i(i+1)}$, $i = 2$ to $N-1$. All other β_{ij} values can be computed from these using (24).

Geometric relations among D_{ij} can be determined from angles β_{ij}. Only one degree of freedom is available for D_{ij} as demonstrated below. Consider the geometric relations shown in Fig. 4, and according to the cosine law,

$$D_{1j} = \frac{\sin(\psi_{1,2,j})}{\sin(\psi_{1,j,2})} D_{12}. \tag{25}$$

Then,

$$D_{ij} = \frac{\sin(\psi_{i,1,j})}{\sin(\psi_{1,i,j})} D_{1j} = \frac{\sin(\psi_{i,1,j})\sin(\psi_{1,2,j})}{\sin(\psi_{1,i,j})\sin(\psi_{1,j,2})} D_{12} \tag{26}$$

Equivalently, we can have

$$D_{ij} = G_{ij} \cdot D_{12} \tag{27}$$

where

$$G_{ij} = \begin{cases} \sin(\beta_{2j} - \beta_{12})/\sin(\beta_{2j} - \beta_{1j}) & \text{, when } i = 1 \\ (\sin(\beta_{1j} - \beta_{1i})\sin(\beta_{2j} - \beta_{12}))/(\sin(\beta_{ij} - \beta_{1i})\sin(\beta_{2j} - \beta_{1j})) & \text{, otherwise} \end{cases}$$

Consequently, the position of each sensor relative to sensor 1 can be derived from D_{12} and β_{ij}. These geographic relations are fundamental to the calibration, as well as to the consistency check algorithm described in the following context.

4. The calibration method

The objective of calibration is to reduce the systematic errors by correcting sensor configuration parameters. Eqs. (18) and (24) can be adopted to determine the angular parameters (ϕ_i and β_{ij}). The distances among sensors can then be computed by (27) given one distance measurement between a pair of sensors. In other words, if that distance measurement and all sensor readings are accurate, then self-calibration can be performed without using external reference measurements. M sets of measurements can be collected by moving the sensor module M times in a homogeneous path (e.g., an arc or a line), and accumulating the data at each movement. These M sets of measurements are denoted as the following vector,

$$X_m = [\bar{x}_{1,m} \quad \bar{y}_{1,m} \quad \bar{x}_{2,m} \quad \bar{y}_{2,m} \quad \cdots \quad \bar{x}_{N,m} \quad \bar{y}_{N,m}]^T, \quad m = 1, 2, \ldots, M \tag{28}$$

Accumulated data can be used instead of a single set of sample data, thus preventing quantization error. The trajectory of the sensor motion is designed such that the vector X_m, $m = 1$ to M, spans the remaining subspace (a condition similar to persistence excitation).

As described in Section 3, the independent angular parameters are ϕ_i's, $i = 2$ to N, β_{1j}, $j = 2$ to N and $\beta_{k(k+1)}$, $k = 2$ to $N-1$. The total number is $(N-1)+(N-1)+(N-2) = 3N-4$. Let Z be the vector

$$Z = [z_1 \quad z_1 \quad \cdots \quad z_{3N-4}]^T = [\phi_2 \quad \phi_3 \quad \cdots \quad \phi_N \quad \beta_{12} \quad \beta_{13} \quad \cdots \quad \beta_{1N} \quad \beta_{23} \quad \beta_{34} \quad \cdots \quad \beta_{(N-1)N}]^T.$$

The problem of solving Z can be cast as the following optimization problem,

$$\underset{Z}{Min}(X_1^T \boldsymbol{B}(Z)^T \boldsymbol{B}(Z) X_1 + X_2^T \boldsymbol{B}(Z)^T \boldsymbol{B}(Z) X_2 + \cdots + X_M^T \boldsymbol{B}(Z)^T \boldsymbol{B}(Z) X_M) \tag{29}$$

This unconstraint optimization problem can be solved by mathematical tools to obtain the angular parameters.The distance among sensors can be calculated from (27) with the calibrated values of the angles if D_{12} is known. Additionally, D_{12} can be calibrated if an external angular measurement is available, as demonstrated below. Substituting (27) into (4) yields

$$\Delta\theta_{ij} = \frac{\sqrt{l_i^2 + l_j^2 - 2\cos(\gamma_{ij}) l_i l_j}}{D_{12} G_{ij}} sign(l_j \sin(\alpha_j + \sigma_{ji}) - l_i \sin(\alpha_i + \sigma_{ij}))$$

For the kth set of data, define a new variable u_k as,

$$u_k = \frac{2}{N(N-1)} \sum_{i=1}^{N-1} \sum_{j=i+1}^{N} \left(\frac{\sqrt{l_{i,k}^2 + l_{j,k}^2 - 2\cos(\gamma_{ij}) l_{i,k} l_{j,k}}}{G_{ij}} \right. \left. sign(l_{j,k} \sin(\alpha_{j,k} + \sigma_{ji}) - l_{i,k} \sin(\alpha_{i,k} + \sigma_{ij})) \right) \tag{30}$$

Therefore, the product of u_k and inverse of D_{12} is equal to average of the orientation estimation of each sensor pair. More precisely,

$$u_k \cdot D_{12}^{-1} = \frac{2}{N(N-1)} \sum_{i=1}^{N-1} \sum_{j=i+1}^{N} \Delta\theta_{ij,k} = \Delta\theta_{\text{real},k} \tag{31}$$

where $\Delta\theta_{\text{real},k}$ denotes the real rotation angle of each set. By collecting K sets of data, the equation can be set as:

$$\boldsymbol{u} \cdot D_{12}^{-1} = \boldsymbol{\theta}_{\text{real}} \tag{32}$$

where $\boldsymbol{\theta}_{\text{real}} = [\Delta\theta_{\text{real},1} \ \Delta\theta_{\text{real},2} \ \ldots \Delta\theta_{\text{real},K}]^T$ is the desired rotation vector, and $\boldsymbol{u} = [u_1 \ u_2 \ \ldots \ u_K]^T$. Finally, this equation can be solved by the least-squares method, as

$$D_{12} = \frac{1}{(\boldsymbol{u}^T \boldsymbol{u})^{-1} \boldsymbol{u}^T \cdot \boldsymbol{\theta}_{\text{real}}} \tag{33}$$

5. Consistency check strategy

The performance of an optical flow sensor depends on the condition of sensing surface. A highly reflective surface or a sudden change of height might seriously disturb the sensor measurements. The influence of distance from surface and different sensing surface type has been addressed in Refs. [9,13,14]. Each pair of sensors

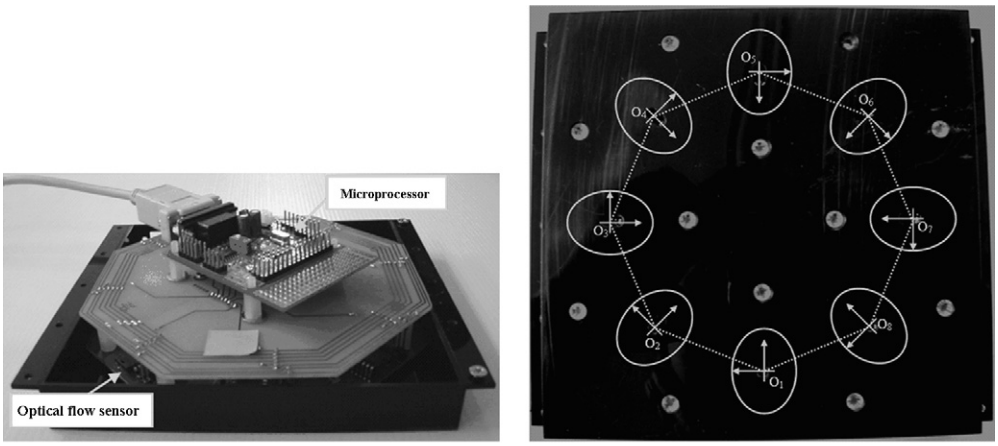

(a) Overall view (b) Bottom view

Fig. 5. The module with eight optical flow sensors.

can estimate the position and orientation according to (1) to (11). For N sensors, $N(N-1)/2$ estimations are provided. To reduce the uncertainty caused by the non-systematic errors, unreliable sensor measurements are removed, and remaining measurements are used to update the position and orientation of the robot as described previously in (12) and (13).

From (18), $\boldsymbol{\varepsilon} = 0$ if the sensor measurements contain no errors. This means that the correct measurement vector X should lie in the null space of the matrix $\mathbf{B}$ (denoted as $\boldsymbol{N}(\mathbf{B})$). Therefore, for any vector X not in $\boldsymbol{N}(\mathbf{B})$, the orthogonal projection of X onto $\boldsymbol{N}(\mathbf{B})$, denoted as X_p, can be interpreted as the consistent part of X, while the projection error, $X_o \equiv X - X_p$, is considered as the inconsistent part. Let

$$X_p = [\bar{x}_{p,1} \quad \bar{y}_{p,1} \quad \bar{x}_{p,2} \quad \bar{y}_{p,2} \quad \cdots \quad \bar{x}_{p,N} \quad \bar{y}_{p,N}]^T \text{ and } X_o = [\bar{x}_{o,1} \quad \bar{y}_{o,1} \quad \bar{x}_{o,2} \quad \bar{y}_{o,2} \quad \cdots \quad \bar{x}_{o,N} \quad \bar{y}_{o,N}]^T$$

The *inconsistency factor* is defined as,

$$\eta_N \equiv \frac{1}{N}\sum_{i=1}^{N}\left(\frac{||X_{o,i}||}{||X_{p,i}||}\right) \tag{34}$$

where $X_{p,i} \equiv [x_{p,i}\, y_{p,i}]^T$ and $X_{o,i} \equiv [x_{o,i}\, y_{o,i}]^T$ are the *consistent* and *inconsistent* parts of each sensor i, respectively. The inconsistent part contains both the measurement noise and false information, as mentioned above. Under normal conditions, only measurement noise will appear in the signal. Therefore, the maximum acceptable inconsistency factor can reasonably be assumed to be related to the statistical property of the measurement noise. This assumption is adopted to determine whether any sensors are unreliable. If the inconsistency factor exceeds a certain threshold, one or more sensor measurements should be rejected. A simple iterative algorithm can be built by removing unreliable sensors one-by-one until the factor η_N is below that threshold. Denoting the threshold as TH_c, the iterative procedure is explained as follows. In this procedure, the measurement vector at sampling time k is denoted as X_k:

(1) Let $N_r = N$ and $X_r = X_k$.
(2) Compute the inconsistency factor η_{N_r} from (34) and if $\eta_{N_r} \leq TH_c$, then stop. Otherwise, continue.
(3) Compute the inconsistency factor $\eta_{N_r-1}(i)$ of the $N_r - 1$ sensors measurements by removing the ith sensor, $i = 1$ to N_r.
(4) Find sensor i that produces the minimum value of $\eta_{N_r-1}(i)$, $i = 1$ to N_r. Remove sensor i from the N_r sensors.
(5) Let $N_r = N_r - 1$. If $N_r = 1$, then stop, otherwise construct the measurement vector X_r of the remaining sensors. Go to step 2.

Notably, the minimum number of sensors required to give a full measurement is 2. If the algorithm stops at $N_r = 1$, then no sensor can be trusted. Furthermore, computing every $\boldsymbol{N}(\mathbf{B}_r)$ at each iteration is unnecessary, because $\boldsymbol{N}(\mathbf{B}_r)$ values can be computed and stored in advance. Following these steps yields the reliable sensor measurements at k. Additionally, the reserved X_r can be adopted as the data set to compute the movement according to (1)–(11), and to update the overall position and orientation by computing the mean of these movements by (12) and (13).

6. Experimental results

A module with eight optical flow sensors was developed, as shown in Fig. 5. The module contained a microprocessor to access data of all sensors simultaneously, and to send the data to a PC via RS-232 at each sample time. The module employed ADNS-6010 type optical flow sensors, manufactured by Avago Technologies.

Table 1
The nominal (with and without 2% variation added) and calibrated parameters (unit: D_{12} mm, ϕ_i degrees, and β_{ij} degrees).

	D_{12}	ϕ_1	ϕ_2	ϕ_3	ϕ_4	ϕ_5	ϕ_6	ϕ_7	ϕ_8	β_{12}	β_{13}
Nominal parameters without variation	37.12	0	45	90	135	180	225	270	315	22.5	45
Nominal parameters with added variation	36	0	44.27	92.77	133.77	179.21	224.71	262.85	316.56	22.12	44.47
Calibrated parameters	37.28	0	47.09	90.70	134.74	180.11	226.28	269.71	314.02	21.40	44.14

	β_{14}	β_{15}	β_{16}	β_{17}	β_{18}	β_{23}	β_{34}	β_{45}	β_{56}	β_{67}	β_{78}
Nominal parameters without variation	67.5	90	112.5	135	157.5	67.5	112.5	157.5	−157.5	−112.5	−67.5
Nominal parameters with added variation	66.84	88.83	111.60	136.44	158.09	66.16	114.24	151.60	−160.92	−110.41	−69.85
Calibrated parameters	66.84	90.39	112.81	135.89	156.22	66.91	112.42	158.73	−154.56	−115.96	−64.85

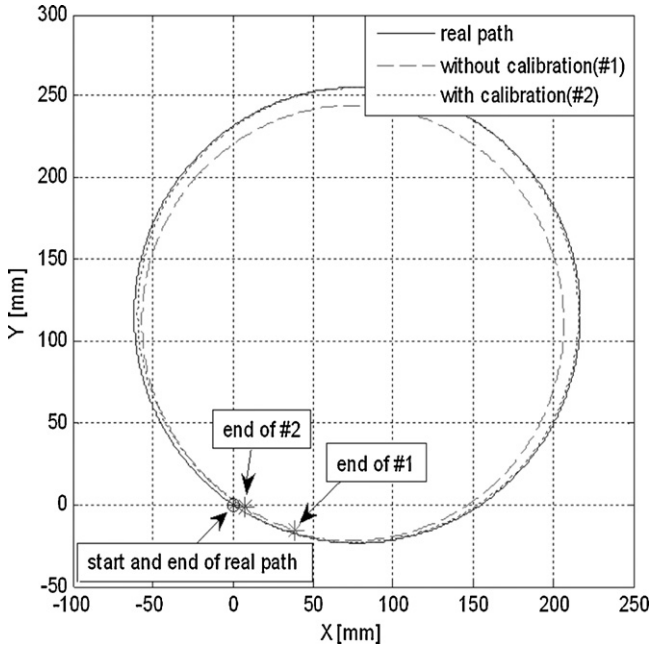

Fig. 6. Localization results with and without using calibrated arguments.

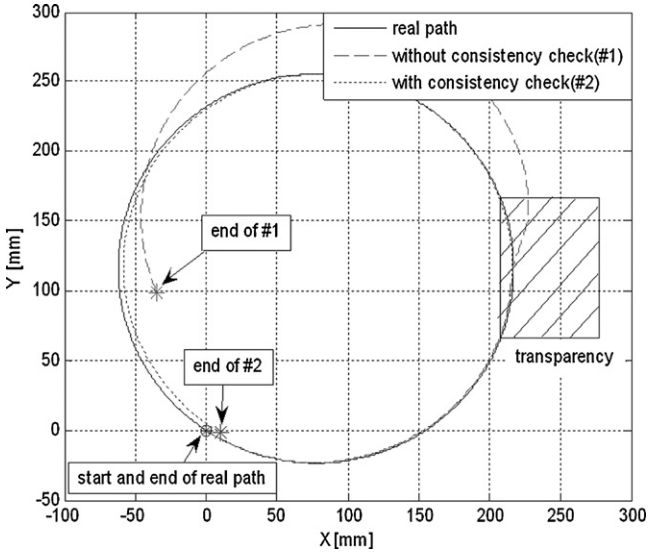

Fig. 7. Localization results with and without using consistency check strategy.

This laser-based type sensor [13] is better than common optical sensors [14], since it is more accurate, less sensitive to height, and capable of measurement at higher speeds. These eight sensors were located at the corners of an octagon, which had a diagonal distance of 97 mm. Therefore, distance between two adjacent sensors was $D_{i(i+1)} = 37.12$ mm, $i = 1$ to 7 (see Fig. 1). The relative orientation between two adjacent sensors was 45°. All independent angles ϕ_i and β_{ij} were determined by assigning the orientation of the coordinate of sensor 1 as the robot coordinate (see Sections 2 and 3). To verify the calibration method proposed in Section 4, a 2% variation was added to the nominal value of each D_{ij}, ϕ_i and β_{ij}. These nominal values were also used as the initial estimate of the optimization problem of (29).

To collect data for calibration, the sensor module was moved along three circles of different radii (80, 92 and 140 mm). Each circle was traversed three times. The CPI (counts per inch) of each sensor was different due to manufacturing variation. Previous studies

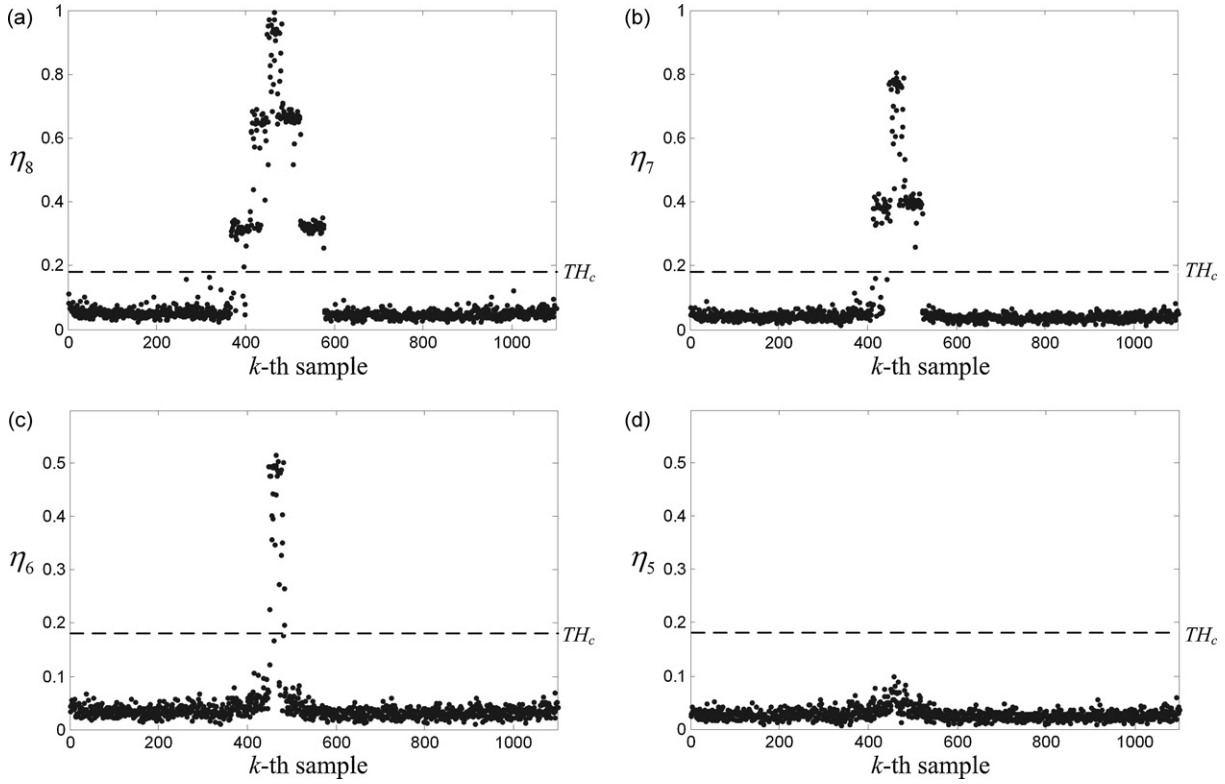

Fig. 8. The details of the consistency check strategy adopted in the experiment using transparency to produce sensor faults: the value of inconsistency factor for (a) all sensors; (b) removing one sensor measurements; (c) removing two sensor measurements; (d) removing three sensor measurements.

have revealed that CPI could also depend on the moving direction or arc displacement radius [9]. This effect was not considered in this work. Instead, the collected data were employed to calibrate the CPI of each sensor according to the distance of travel. The accumulated data were used to solve the angular parameters using (29) by MATLAB (a built-in function named *fminunc*). Once angular parameters were obtained, the same accumulated data with a 360° rotation was used to calculate the distance D_{12} as (33). Table 1 shows the nominal (with and without 2% variation added) and calibrated parameters. These calculation results indicate that the variation decreased, meaning that the calibration method was effective. The parameters with and without calibration were used to compute the trajectory by traveling the module along the circle of 140 mm radius. Fig. 6 shows the results of this calculation, where the calibrated sensor produced an error of 2.49 mm when returning to the starting point.

To show the effectiveness of the consistency check strategy described in Section 5, the module was moved along the same path with a piece of rectangular transparency occupying a portion of the path. The ratio of the standard deviation to the mean of the sensor measurement under normal condition was obtained in advance, and found to be 0.0113. The threshold TH_c was set to 16 times of the ratio (i.e., $TH_c = 0.1808$). As shown in Fig. 7, the trajectory computation that did not implement the consistency check strategy changed suddenly when the transparency was passed, resulting in a large error. In contrast, the computation using the strategy described in Section 5 successfully eliminated the faulty sensors, and produced more accurate estimations than the case without using the strategy. The error at returning to the end point was 5.7 mm, producing an accuracy of 0.65% for traveling along the circle. The sampling period where 1–3 sensors (sensor number 1, 7 and 8) passed by the transparency demonstrates the effect of the consistency check strategy. Fig. 8 shows that during this period, the inconsistency factor grows above the threshold without removing the faulty measurements. Correct results were obtained when implementing the proposed method in Section 5.

7. Conclusion

This work proposes an odometer with multiple optical flow sensors. Since the relative positions of the sensors are unchanged, their measurements should obey the rigid-body constraint, i.e., the projections of velocity measurements of a pair of sensors onto the line connecting them should be equal. This relation is first applied to calibrate the parameters of sensor configuration. Analytical results show that all parameters can be computed from the sensor measurements and the rotation angle of the module. To filter out incorrect sensor data during operation, the rigid-body constraint is again used to construct the null space containing the sensor data vector. The reliability of the sensor data is assessed from the distance to the null space. Experiments are conducted to support the proposed methods, and experimental results show that the proposed methods are more accurate than existing ones.

Acknowledgments

This work was supported in part by the National Science Council of the Republic of China, Taiwan for financially supporting this research under contract number NSC 95-3113-P-009-003 as well as the Precision Machinery Center of Taiwan under contract number 96TR04.

References

[1] J. Borenstein, H.R. Everett, L. Feng, Navigating Mobile Robots: Sensors and Techniques, A.K. Peters, Wellesley, MA, 1996.
[2] J. Borenstein, L. Feng, Measurement and correction of systematic odometry errors in mobile robots, IEEE Transactions on Robotics and Automation 12 (6) (1996) 869–880.
[3] D.K. Sorensen, V. Smukala, M. Ovinis, S. Lee, On-line optical flow feedback for mobile robot localization/navigation, in: IEEE/RSJ International Conference on Intelligent Robots and Systems, Las Vegas, Nevada, October, 2003, pp. 1246–1251.
[4] S. Lee, J.B. Song, Robust mobile robot localization using optical flow sensors and encoders, in: IEEE International Conference on Robotics and Automation, New Orleans, LA, April, 2004, pp. 1039–1044.
[5] S. Lee, J.B. Song, Mobile robot localization using optical mice, in: IEEE International Conference on Robotics, Automation and Mechatronics, Singapore, December 1–3, 2004, pp. 1192–1197.
[6] D. Sekimori, F. Miyazaki, Self-localization for indoor mobile robots based on optical mouse sensor values and simple global camera information, in: IEEE International Conference on Robotics and Biomimetics, 2005, pp. 605–610.
[7] A. Bonarini, M. Matteucci, M. Restelli, Automatic error detection and reduction for an odometric sensor based on two optical mice, in: IEEE International Conference on Robotics and Automation, Barcelona, Spain, April, 2005, pp. 1675–1680.
[8] A. Bonarini, M. Matteucci, M. Restelli, A kinematic-independent dead-reckoning sensor for indoor mobile robotic, in: IEEE/RSJ International Conference on Intelligent Robots and Systems, Sendai, Japan, September 28–October 2, 2004, pp. 3750–3755.
[9] J. Palacin, I. Valgañon, R. Pernia, The optical mouse for indoor mobile robot odometry measurement, Sensors and Actuators A: Physical 126 (2006) 141–147.
[10] J.-S. Hu, J.-H. Cheng, Y.-J. Chang, Spatial trajectory tracking control of omni-directional wheeled robot using optical flow sensors, in: 1st IEEE Multi-conference on Systems and Control, Singapore, October 1–3, 2007, pp. 1462–1467.
[11] J.-S. Hu, Y.-J. Chang, W.-H. Liu, C.-H. Yang, Localization of an omni-directional robot platform using sound field characteristics and optical flow sensing, in: International Conference on Advanced Robotics, August 21–24, 2007.
[12] G.B. Gordon, D.L. Knee, R. Badyal, J.T. Hartlove, Proximity detector for a seeing eye mouse, United States Patent No. 6281882, August 28, 2001.
[13] Datasheet, ADNS-2051 Optical Mouse Sensor, Agilent Technologies, 2004.
[14] Datasheet, ADNB-6011-EV and ADNB-6012-EV High Performance Laser Mouse Bundles, Avago Technologies, 2006.

Biographies

Jwu-Sheng Hu received the B.S. degree from the Department of Mechanical Engineering, National Taiwan University, Taiwan, in 1984, and the M.S. and Ph.D. degrees from the Department of Mechanical Engineering, University of California at Berkeley, in 1988 and 1990, respectively. He is currently a Professor in the Department of Electrical and Control Engineering, National Chiao-Tung University, Taiwan, R.O.C. His current research interests include microphone array signal processing, active noise control, intelligent mobile robots, embedded systems and applications.

Yung-Jung Chang received the B.S. degree from the Department of Electrical Engineering, Yuan-Ze University, Taiwan, R.O.C., and the M.S. degree from the Department of Control Engineering, National Chiao-Tung University (NCTU), Taiwan, R.O.C., in 2005 and 2006, respectively. He is currently working toward the Ph.D. degree at NCTU. His research interests are mobile robot localization and navigation.

Yu-Lun Hsu received the B.S. degree from the Department of Electrical Control Engineering, National Chiao-Tung University (NCTU), Taiwan, R.O.C., in 2007. He is currently working toward the M.S. degree at NCTU. His major interests are image processing.